Weierstraß-Institut
für Angewandte Analysis und Stochastik
Leibniz-Institut im Forschungsverbund Berlin e. V.

Reduced-order unscented Kalman filter in the frequency domain: Application to computational hemodynamics

Lucas O. Müller[1], Alfonso Caiazzo[2], Pablo J. Blanco[3]

submitted: February 27, 2018

[1] Norwegian University of Science and Technology (NTNU)
Richard Birkelands vei 1A
7491 Trondheim, Norway
E-Mail: lucas.o.muller@ntnu.no

[2] Weierstrass Institute
Mohrenstr. 39
10117 Berlin, Germany
E-Mail: alfonso.caiazzo@wias-berlin.de

[3] National Laboratory for Scientific Computing (LNCC)
Av. Getúlio Vargas 333, Quitandinha
CEP 25651-075 Petrópolis (RJ), Brazil
E-Mail: pjblanco@lncc.br

No. 2484

Berlin 2018

Reduced-order unscented Kalman filter in the frequency domain: Application to computational hemodynamics

Lucas O. Müller, Alfonso Caiazzo, Pablo J. Blanco

Abstract

Objective: The aim of this work is to assess the potential of the reduced order unscented Kalman filter (ROUKF) in the context of computational hemodynamics, in order to estimate cardiovascular model parameters when employing real patient-specific data. Methods: The approach combines an efficient blood flow solver for one-dimensional networks (for the forward problem) with the parameter estimation problem cast in the frequency space. Namely, the ROUKF is used to correct model parameter after each cardiac cycle, depending on the discrepancies of model outputs with respect to available observations properly mapped into the frequency space. Results: First we validate the filter in frequency domain applying it in the context of a set of experimental measurements for an in vitro model. Second, we perform different numerical experiments aiming at parameter estimation using patient-specific data. Conclusion: Our results demonstrate that the filter in frequency domain allows a faster and more robust parameter estimation, when compared to its time domain counterpart. Moreover, the proposed approach allows to estimate parameters that are not directly related to the network but are crucial for targeting inter-individual parameter variability (e.g., parameters that characterize the cardiac output). Significance: The ROUKF in frequency domain provides a robust and flexible tool for estimating parameters related to cardiovascular mathematical models using in vivo data.

1 Introduction

One-dimensional hemodynamic models provide a powerful tool for the computational simulation of blood flow in the cardiovascular system. These models have been used for providing useful insight in the understanding of cardiovascular physiology and pathology (see, e.g., [13, 8, 21, 17, 3]) and they have been deeply validated versus in vitro experiments (see, e.g., [15]) and in vivo measurements (see, e.g., [4, 22, 20]).

In order to enhance the predictive and descriptive capabilities of one-dimensional (1D) models in clinically relevant applications, it is highly desirable to have a framework that allows to tune geometrical and physical parameters of the mathematical model in order to achieve patient-specific simulations, i.e., to be able to accurately predict the hemodynamics in specific subjects. This is the focus of data assimilation and parameter estimation methods, that is, algorithms that combine available measurements with mathematical models in order to improve the accuracy of model predictions.

In particular, the reduced-order unscented Kalman filter (ROUKF) (see, e.g., [11, 10, 16]) is a sequential data assimilation approach in which the computed state and the estimates for model parameters are corrected at each time step of the simulation, taking into account the error between the available measurements and the current numerical predictions. One of the main advantages of the ROUKF is that it does not require the solution of a tangent problem in order to compute the optimal estimates, as it is based on an efficient sampling of the parameter space.

The ROUKF applied to 1D computational hemodynamics was reported for the first time in [14], using only synthetic data, i.e., where full field (pressure and flow rate) measurements along the definition of the whole continuum were generated by the same mathematical model and employed as observations. An assessment considering more realistic (in vitro) observational data was discussed in [6], from where it was concluded about the real potential of the ROUKF in clinically relevant scenarios, identifying, at the same time, the high sensitivity of results with respect to the quality of measurements. Recently, an approach based on the so-called *ensemble Kalman filter*, in combination with lumped (0D) cardiovascular models, has been investigated in [12]. Up to our knowledge, parameter estimation for one-dimensional models and using in vivo data has not been addressed yet.

Naturally, the ROUKF is formulated in the time domain. The main goal of the present work is to present a reformulation of the ROUKF to be applied to hemodynamic problems in which available measurements belong to the frequency domain. The approach is motivated by the fact that clinical measurements are often related to maximum/minimum values, average values, frequency spectra or any other features retrieved from signals (e.g. pressure and flow rate signatures) throughout the cardiac cycle. We assume quasi-periodicity of data, which is reasonable because most acquisition techniques are based on averaging the data through several cardiac cycles. Hence, we will show that the formulation in frequency space provides a more robust data assimilation with respect to the classical time domain counterpart, suitable for parameter estimation utilizing in vivo patient data. To this aim, we use the ROUKF in combination with an efficient parallel explicit solver for blood flow in one-dimensional networks [18] that allows for extremely fast forward simulations, and, consequently, for reasonable computational times when considering parameter estimation taking up to several hundreds of cardiac cycles.

Moreover, to validate the filter in the frequency domain, we first consider an estimation experiment based on in vitro data, using the arterial network model described in [15, 1], for which parameter values have been carefully measured, and, at the same time, experimental flow and pressure measurements are available at selected points over the network (at most one measurement location per vessel). For this setting, the results are compared with the results of the time-domain ROUKF as reported in [6]. Next, we employ in vivo patient data reported by [22] to perform the estimation of parameters for the underlying one-dimensional model.

In both cases (in vitro and in vivo), we present different sets of numerical tests to investigate the accuracy and robustness of the proposed strategy, comparing the results with the classical ROUKF in the time domain. In the in vitro case, we focus on the estimation of terminal resistances used for imposing boundary conditions and on the estimation of arterial wall parameters (such as Young's modulus and vessel wall thickness). When considering in vivo measurements, we address the estimation of vessel compliances and parameters that shape the cardiac output inflow waveform. Noteworthy, and unlike the time domain ROUKF, the latter case can straightforwardly be implemented in the frequency domain.

2 Methods

2.1 One-dimensional blood flow model

One-dimensional models are a suitable approach to investigate wave propagation phenomena in large arterial and venous networks. These models deliver valuable information on pressure and flow wave-

forms, while keeping the computational cost reasonably low. The set of equations under study is

$$\begin{cases} \dfrac{\partial A}{\partial t} + \dfrac{\partial q}{\partial x} = 0, \\[2mm] \dfrac{\partial q}{\partial t} + \dfrac{\partial}{\partial x}\left(\dfrac{q^2}{A}\right) + \dfrac{A}{\rho}\dfrac{\partial p}{\partial x} = f, \end{cases} \tag{1}$$

where $A(x,t)$ is the cross-sectional area, $q(x,t)$ is the mass flow rate, $p(x,t)$ the average blood pressure over the cross section, $f(x,t)$ stands for the friction force per unit length and ρ denotes the blood density. We close system (1) taking $f = -\frac{8\pi\mu}{\rho}\frac{q}{A}$ (μ the dynamic viscosity of blood), and introducing a constitutive law (usually called *tube law*) that relates the strain and strain rate of the vessel wall to the internal pressure [1] via the following relation

$$p = \frac{\beta}{A_0}(\sqrt{A} - \sqrt{A_0}) + \frac{\Gamma}{A_0\sqrt{A}}\frac{\partial A}{\partial t}, \tag{2}$$

with

$$\beta = \frac{4}{3}\sqrt{\pi}Eh, \quad \Gamma = \frac{2}{3}\sqrt{\pi}\Phi h, \tag{3}$$

where Φ is the viscosity of the vessel wall, E is its Young's modulus, h is the wall thickness and A_0 is a reference cross-sectional area of the vessel.

Boundary conditions at vessels ends can be of different nature. One can prescribe boundary conditions, for example a pressure or flow rate waveform prescribed at the inlet of the network. Also, vessels can be coupled to other vessels via appropriate junction conditions. In addition, at terminal sites, vessels can be coupled to lumped parameter models representing the peripheral circulation (see, e.g., [7]).

The parameter identification technique used in this paper requires the approximate solution of the direct problem, i.e., equations (1) and (2). Therefore, the numerical method used for this application must be efficient and robust, as well as numerically consistent and stable. Efficiency is mandatory since the solution of inverse problems requires multiple solutions (e.g., several cardiac cycles for several instances) of the forward model. Robustness is necessary in the sense that the numerical scheme must be able to admit sudden and large variations of parameters, induced by the filter correction at each iteration (see Section 2.2 for details). Here we use a local time stepping finite volume numerical scheme [18], which has shown to possess the above mentioned features. This scheme is based on the ADER (Arbitrary high-order DERivative Riemann problem) methodology, which allows for arbitrary accuracy in space and time (see [25, 24] for a detailed introduction). However, any other numerical scheme for one-dimensional blood flow models satisfying such requirements could equally be employed.

2.2 The reduced-order unscented Kalman filter

The Kalman filter is a widely used tool for data assimilation applications, improving of model predictions by estimating the values of unknown parameters, taking into account available measurements on a given system (see, e.g., [16]).

The purpose of this section is to provide a short derivation of the method, focusing on the most relevant practical aspects concerning the application to one dimensional blood flow models. We refer, e.g., to [27] for a more detailed description.

Let us write the discretized counterpart of the one-dimensional evolution model described in Section 2.1 in the form of a dynamical system

$$X_{n+1} = \mathcal{F}(X_n, \theta) \tag{4}$$

(equipped with a proper initial condition), where X_n contains the *state variables* at time step t_n (values of flow, pressure and cross-sectional area at each discretization node along the network and state variables of the lumped parameter models), $\mathcal{F}$ is an operator which depends on equations (1) and on their particular discretization, and θ is a vector of *parameters*, whose values are to be estimated. For instance, these unknown parameters might comprise the Young's modulus of selected vessel segments or the terminal resistances of lumped parameter models.

Let us now assume that a measurement vector $Z_n \in \mathbb{R}^M$, for M measurements, is available at $n = 1, \dots, N$ selected time instants, obtained by observing the state X through an *observation* operator $\mathcal{H}_n(X_n)$, such that

$$Z_n = \mathcal{H}_n(X_n) + \xi^Z \,, \tag{5}$$

affected by a noise ξ^Z, usually assumed to be independent at all times and Gaussian with zero-mean. For simplicity, let us assume that the observation operator is linear, i.e., $\mathcal{H}_n(X_n) = H_n X_n$. In a clinical setting, the main contribution to the observation noise is given by error statistics of measurement devices.

2.2.1 The least-squares approach

The goal of data assimilation is to find, in the least-squares sense, the best guess of the true value of the unknown state. In what follows, the state computed through the computational model will be denoted with X, while the corrected state will be denoted with $\hat{X}$.

This state can be defined introducing the scalar cost-function

$$J(\hat{X}) = \xi^Z W^{-1} \xi^Z = [Z - H\hat{X}] W^{-1} [Z - H\hat{X}] \,, \tag{6}$$

which depends on the difference between the measurements and the output of the observation operator applied to the estimate and on a weighting matrix W, which can be related to the confidence on the measurements Z. The optimal state can be computed as $\hat{X} = \left(H^T W^{-1} H \right)^{-1} H^T W^{-1} Z$.

The solution $\hat{X}$ is usually called the *estimator*. However, when the number of measurements becomes large, e.g., for time dependent problems, the previous optimal least-squares formula becomes rather inefficient from the computational point of view.

In these cases, a suitable alternative consists in a *sequential* approach, i.e., an iterative strategy that computes the optimal state $\hat{X}_n$ at time step n based on the previously computed estimates and on the latest measurement errors. This approach can be written in the general form

$$\begin{aligned} Z_n &= H_n X_n + \xi_n, \\ \hat{X}_n &= X_n + K_n \left(Z_n - H_n X_n \right), \end{aligned} \tag{7}$$

where the matrix K_n, referred to as the *filter* (or gain), should be designed in such a way to reduce the error $\varepsilon_{X,n} = X - \hat{X}_n$ (in a given norm) when taking into account Z_n.

Let us now introduce the matrix $P_k = \mathbb{E}\left[\varepsilon_{X,k}\, \varepsilon_{X,k}^T\right]$ representing estimation error covariance and a time dependent confidence matrix W_k. The following proposition holds:

Proposition 1: *Let $\hat{X}_0 = X$ and let us assume that the measurement noise has zero mean, i.e. that it holds $\mathbb{E}[\xi_k] = 0$. Then the filter can be defined at each step as*

$$K_k = P_{k-1} H_k^T \left(H_k P_{k-1} H_k^T + W_k \right)^{-1} \,.$$

See [27] for a detailed proof.

The idea behind the Kalman filter is to consider an augmented state (X_n, θ_n), including a trivial dynamics for the parameters, i.e., assuming that they do not change in time. Namely, a prediction is obtained via a forward propagation

$$
\begin{aligned}
X_{n+1}^- &= \mathcal{F}(X_n^+, \theta_n)\,, \\
\theta_{n+1}^- &= \theta_n\,,
\end{aligned}
\tag{8}
$$

while the correction takes into account the discrepancies between observations and measurements

$$
\begin{aligned}
X_{n+1}^+ &= X_{n+1}^- + K_X \left(Z_{n+1} - H_{n+1} X_{n+1}^- \right)\,, \\
\theta_{n+1}^+ &= \theta_{n+1}^- + K_\theta \left(Z_{n+1} - H_{n+1} X_{n+1}^- \right)\,.
\end{aligned}
\tag{9}
$$

The *Kalman matrices* K_X and K_θ are defined in order to minimize the distance between observations and measurements in a proper norm, which depends on the confidences in both the measures and the model.

2.2.2 The unscented Kalman filter

It can be shown that, in the case of linear dynamics with white noise, the Kalman filter provides an optimal estimate [16]. For non-linear systems, different extensions of the Kalman filter are available. Among these, the unscented Kalman filter (UKF) achieves second order accuracy employing a minimal set of deterministically chosen points in the state space for forward propagation [26].

In this case, the prediction-correction strategy for the filtering consists in (i) a forward propagation of the mean (current estimate) and covariance of the state, based on the dynamics of selected points in the state space, and in (ii) a correction of the propagated statistics, computed taking into account the noisy observations. In particular, the UKF computes state and parameter estimates at all time steps, as well as estimators for state and parameter covariance matrices, based on the current iteration and on the observation noise covariance W.

The UKF might involve costly operations on large matrices (dimension of the state vector). However, neglecting the uncertainty on the state (i.e. on the initial conditions) allows to formulate the so-called *reduced-order* unscented Kalman filter (ROUKF) [16], for which inversion is only required for matrices of the size of the unknown parameter space. Moreover, the estimation of p parameters can be efficiently performed with a discretization containing only $p+1$ points for the state-parameter space (see, e.g., [16, 9] for details), which is also called simplex *sigma-points*. For simplicity of notation, in what follows the $p+1$ sigma-points will be grouped in a matrix $\mathcal{I} \in \mathbb{R}^{(p+1) \times p}$, while the weights will be collected in a diagonal matrix D.

The estimation via ROUKF can be summarized by the following steps (see, e.g., [16, 27, 2] for further details):

- Initialization: Assume that the initial estimates X_0 and θ_0, are given, and initialize the matrix

$$
U_0 = (P^\theta)^{-1} = \mathrm{diag}\left\{ \frac{1}{\sigma_{\mathrm{par},1}^2}, \frac{1}{\sigma_{\mathrm{par},2}^2}, \ldots, \frac{1}{\sigma_{\mathrm{par},p}^2} \right\}
$$

  as the inverse of the diagonal covariances for each parameter. The values $\sigma_{\mathrm{par},1}, \ldots, \sigma_{\mathrm{par},p}$ control the confidence in the initial guess for the parameters (larger values indicate less confidence in the initial estimates). Set the initial error covariance estimator as

$$
L_0^\theta = \mathbb{I}_{p \times p}, \ L_0^X = \mathbf{0}_{n_x \times p},
$$

where $\mathbb{I}_{p\times p}$ denotes the $p \times p$ identity matrix and $\mathbf{0}_{n_x \times p}$ is a vanishing matrix of the size of state vector. Set $n = 0$.

■ Until convergence, do

■ Sampling: generate the new sigma-points using the current estimates and error covariance estimators:

$$
\begin{aligned}
X_{n,(i)}^+ &= X_n^+ + L_n^X C_n^T \mathcal{I}_{(i)}, \; i = 1, \ldots, p+1 \\
\theta_{n,(i)}^+ &= \theta_n^+ + L_n^\theta C_n^T \mathcal{I}_{(i)}, \; i = 1, \ldots, p+1
\end{aligned}
\tag{10}
$$

where $C_n = \sqrt{U_n^{-1}}$ (Cholesky factorization).

■ Forward propagation:

$$
\begin{aligned}
X_{n+1,(i)}^- &= \mathcal{F}(X_{n,(i)}^+, \theta_{n,(i)}^+), \; i = 1, \ldots, p+1 \\
\theta_{n+1,(i)}^- &= \theta_{n,(i)}^+, \; i = 1, \ldots, p+1 \\
X_{n+1}^- &= \mathbb{E}\big[X_{n+1,(1,\ldots,p+1)}^-\big] \\
\theta_{n+1}^- &= \mathbb{E}\big[\theta_{n+1,(1,\ldots,p+1)}^-\big]
\end{aligned}
\tag{11}
$$

■ Compute

$$
\Gamma_{n+1} = Z_{n+1} - H_{n+1} X_{n+1}^-
\tag{12}
$$

■ Update error covariance estimators:

$$
\begin{aligned}
L_{n+1}^X &= X_{n+1}^- D \, \mathcal{I}^T \\
L_{n+1}^\theta &= \theta_{n+1}^- D \, \mathcal{I}^T \\
L_{n+1}^\Gamma &= \Gamma_{n+1} D \, \mathcal{I}^T \\
U_{n+1} &= \mathcal{I} D \mathcal{I}^T + \big(L_{n+1}^\Gamma\big)^T W_{n+1}^{-1} L_{n+1}^\Gamma
\end{aligned}
$$

■ Correction:

$$
\begin{aligned}
X_{n+1}^+ &= X_{n+1}^- \\
&\quad - L_{n+1}^X U_{n+1}^{-1} \big(L_{n+1}^\Gamma\big)^T W_{n+1}^{-1} \mathbb{E}\left[\Gamma_{n+1}\right] \\
\theta_{n+1}^+ &= \theta_{n+1}^- \\
&\quad - L_{n+1}^\theta U_{n+1}^{-1} \big(L_{n+1}^\Gamma\big)^T W_{n+1}^{-1} \mathbb{E}\left[\Gamma_{n+1}\right],
\end{aligned}
$$

where W_{n+1} denotes the covariance matrix of the measurements. In the numerical studies presented in this paper, W_n was assumed to be diagonal at each measurement time.

The stopping criterion can be defined, e.g., monitoring the RMS deviation of parameters over a cardiac cycle.

2.3 ROUKF in the frequency domain

The goal of this paper is the parameter estimation via Kalman filtering, applied in frequency domain. In order to apply the framework and the algorithm introduced in Section 2.2.2, this approach corresponds to sampling the dynamics with a time step equal to the period of the cardiac cycle and to define the observation operator $\mathcal{H}$ as the magnitude of the discrete Fourier transform (DFT) of selected variables.

The main difference is that, observing the magnitude of the modes in frequency domain, also the measurement noise must be transformed. Let us assume that measurement errors are described by Gaussian, independent random variables at each observation time t_n, i.e., $\xi(t_n) \sim \mathcal{N}(0, \sigma^2)$ for a given variance σ^2. In this case, the Fourier coefficients of $\mathrm{DFT}\,(\xi(t_n))$ are also normally distributed in frequency space, i.e., $a(k) = \mathcal{N}(0, \sigma_{\mathrm{DFT}}^2)$, $b(k) = \mathcal{N}(0, \sigma_{\mathrm{DFT}}^2)$, with variance $\sigma_{\mathrm{DFT}} = \sigma\sqrt{\frac{N}{2}}$, depending on the size of the sample N (in this case, the number of time steps at which measurements are available).

As a consequence, one obtains that the magnitude of the mode related to a frequency k, i.e., $m(k) = \sqrt{a(k)^2 + b(k)^2}$, follows the so-called Rayleigh distribution, for which the expected value and the variance depend on σ^2 (variance of the measurement noise) through

$$\mathbb{E}[m] = \frac{\sigma}{\sqrt{2}}\sqrt{\frac{\pi}{2}}, \ \mathsf{Var}[m] = \frac{4-\pi}{2}\frac{\sigma^2}{2}\,. \tag{13}$$

In view of this fact, we redefine the observation as

$$\hat{Z}_n^j = \mathrm{DFT}^j(H_n X_n) + \hat{\xi}_n^j, \tag{14}$$

where j denotes the j-th mode, and

$$\hat{\xi}_n^j := \mathrm{DFT}^j(\xi_n) - \mathbb{E}[\mathrm{DFT}^j(\xi_n)]\,, \tag{15}$$

where $\mathbb{E}[\mathrm{DFT}^j(\xi_n)]$ is given by (13). This implies that each measurement in time domain results in N_{harm} observations in the frequency domain, where N_{harm} is the number of harmonics that we choose to analyze. This allows for additional flexibility when setting up the filter procedure, e.g., concentrating on average values or on specific modes, depending on the type of observation and on the target parameters.

It is important to note that in (15) we explicitly subtracted the expected value of the resulting distribution for magnitudes. Notice that this value is known, if the variance of the measurement noise is assumed to be known. By construction, one obtains that $\mathbb{E}[\hat{\xi}_n^j] = 0$, for any j. As a consequence, the derivation of the iterative procedure and the optimal filter discussed in Proposition 1 for the time domain can be applied analogously also to the frequency domain.

Notice that in this case the entries of diagonal covariance matrix W_n should be defined using the variance relations specified in (13).

3 Validation: in silico and in vitro data

We consider the in vitro model of the human arterial network described in [15, 1]. Figure 1 shows the vessel network, which is composed of 37 silicone tubes. The network inlet is connected to a pump, mimicking the action of the heart, while terminal vessels are coupled to purely resistive elements, i.e.,

$$q_t = \frac{p_t - P_{\mathrm{res}}}{R_{\mathrm{pher}}}\,, \tag{16}$$

where q_t is the flow rate at the terminal site coming from the 1D model, p_t is the pressure in the 1D model at the terminal site, P_{res} is the residual pressure, which normally models the pressure of the venous system, and R_{pher} is the peripheral resistance.
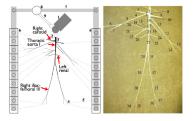
Figure 1: Schematic representation of the in vitro model of the human arterial network presented in [15, 1], reproduced with permission.

This model has been extensively used for validation of numerical approaches (see, e.g., [1, 19]) and to compare results obtained by different numerical methods [5]. This model and the corresponding available data offer the possibility of assessing the Kalman filter in a realistic in vitro setting, in which, at the same time, the uncertainty on model parameters is very low as mechanical and geometrical properties of the vessels that compose the network were carefully measured and reported in the above cited references. The detailed equations and parameters defining the mathematical model, as well as the setup of the considered numerical tests, have been provided as supplementary material to this article.

3.1 Test (E)

Here we consider the estimation of the stiffness of the eight segments describing the aorta (i.e. a single model parameter), comparing the results performing the estimation in frequency and in time domain, and considering available in vitro observation or synthetic data (e.g., data generated by the mathematical model itself). The parameter to be estimated is initialized with a value equal to twice the reference value. It is evident that for the in silico case we expect to retrieve the reference value. The results reported in Figure 2 show that the estimated value $E = 1.28$ MPa - when the filter is applied in frequency domain - is very close to the result of [6] obtained with the estimation in time domain ($E = 1.31$ MPa, less than 3% difference). However, filtering in frequency domain shows a faster convergence.
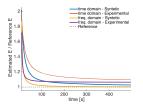

Figure 2: Test (E). Values of the aorta Young modulus during the filter iteration (w.r.t. the reference values provided in [15]) comparing the ROUKF in time and frequency domains, and using synthetic or experimental measurements.

3.2 Test (E+R)

As next, we estimate the stiffness of the eight segments describing the aorta (as a single parameter) and the value of the total resistance of the terminals used for defining the boundary conditions. For

the resistance, the estimation problem has been formulated in terms of an unknown parameter a such that the terminal resistance of vessel i can be written as $R_i = aR_i^{\mathrm{ref}}$, where R_i^{ref} is the value provided in [1]. In both cases, the filter is fed with flow measurements in the aortic arch (vessel 10) , thoracic aorta (17), right iliac femoral artery (30), and right carotid artery (3), and one pressure measurement in the right ulnar artery (7). As in the previous case, the parameters to be estimated are initialized with a value equal to twice the reference value.

Figure 3 shows the variation of the two parameters over time. As in the previous test, the estimated parameters applying the filter in frequency domain ($E = 1.30$ MPa, $a = 1.02$) are very close to the ones obtained with the standard estimation in time domain ($E = 1.32$ MPa, $a = 1.02$). Notice as well that the estimation in frequency domain needs slightly less iterations to converge.
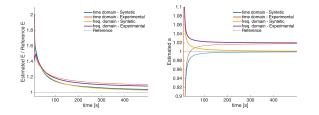

Figure 3: Test (E+R). Top: Values of the aorta Young modulus during the filter iteration (w.r.t. the reference values provided in [15]) comparing the ROUKF in time and frequency domains, and using synthetic or experimental measurements. Bottom: Values of the factor multiplying the terminal resistances during the filter iteration (the unitary value is the reference value).

4   Tests with in vivo measurements

This section focuses on the parameter estimation using real patient measurements. Namely, we consider the ADAN86 arterial circulation model (described in [23]), including the main 86 arteries (see Figure 4, left) and the experimental measures reported in [22][1]. The detailed equations and parameters defining the mathematical model, as well as the setup of the considered numerical tests, have been provided as supplementary material to this article.

In order to show the relevance of filtering parameters in frequency domain, we focus on two sets of parameters that are more relevant for the shape of the pulse wave.

For the different cases, we show the variation of the estimated parameters in time and the errors in frequency space with respect to the observations obtained running a simulation with the new parameters. These errors are computed as the sum of the difference in the k-th harmonic weighted by k^2:

$$e_{FD} = \sqrt{\sum_{k=1}^{N_h} \frac{1}{k^2} \left\| \mathrm{DFT}(Z_k) - \mathrm{DFT}\left(H_n X_n\right)_k \right\|^2}, \tag{17}$$

Notice that (17) neglects the contribution of the discrepancy in the mean value ($k = 0$).

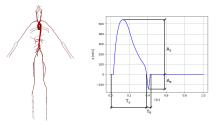[1]Original data has been kindly provided by Dr. P. Reymond.

Figure 4: Left. Schematic representation of the ADAN model. This model has been designed in order to reproduce, within reasonable limits, the predictions of the more complex ADAN model [4] (containing more than 4000 arteries) in terms of main hemodynamic indexes, e.g., flow distribution among organs, mean and pulse pressure values. Right. Inflow profile prescribed at the aortic root, parametrized by systole and backflow amplitudes (A_S and A_B) and durations (T_S and T_B).

4.1 Test (E+C)

In this test we aim at estimating the Young modulus of minor abdominal arteries (E_{abd}), the compliance of the corresponding terminal lumped models (C_{abd}), the Young modulus of lower limbs arteries (E_{lwl}) and the compliance of the corresponding terminal lumped models (C_{lwl}). This amounts to a total of four parameters, using two flow measurements (abdominal and thoracic aorta). In this case, we parametrize the Young modulus of the abdominal and lower limb arteries as $E_i = 2^{\alpha_i} E_{orig}$, where E_{orig} is the *unfiltered* parameter value (initial guess), and α_i ($i \in \{abd, lwl\}$) have to be estimated. The compliance of lumped models for the two different vessel groups are parametrized as $C_i = 2^{\beta_i} C_{orig}$, where C_{orig} is the *unfiltered* parameter value (initial guess), and β_i ($i \in \{abd, lwl\}$) have to be estimated. Notice that, for the estimation, we excluded the first harmonic of the Fourier transform (mean value of the measured signal).

Figure 5 shows the values of the capacitances during the estimation algorithm. In particular, the algorithm converges in a relatively short time (less than 50 iterations), yielding a decrease in the capacitance of the abdominal vessels, and an increase in the lower limb region.
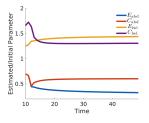

Figure 5: Test (E+C). Values of the estimated parameters during the filter iteration.

As next, we perform a numerical simulation using the filtered parameters. Figure 6 compares the spectrum of the measurements of the original (unfiltered) and filtered settings, showing a considerable improvement in the dominant harmonics. Moreover, it shall be observed that the error in the mean value (0-th harmonic) does not improve, consistently with the fact that this part of the measurement has not been included in the estimation. It is worth mentioning that, in the same setting, the estimation in the time domain failed because, due to large discrepancies between model and data, the filter imposed very large changes to state yielding instability in the one-dimensional blood flow solver.
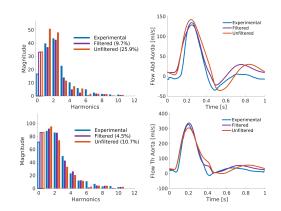
Figure 6: Test (C). Left: Errors in frequency space for the considered measurements. Averaged errors (17) are reported in the legend. The first bar is filled in white in order to highlight that the 0-th harmonic was not used for the estimation. Right: Comparison (in time domain) of measurements with simulation results after filtering. The top row corresponds to the abdominal aorta, while the bottom row refers to the thoracic aorta.

4.2 Test (CERQ)

The second test focuses on estimating systemic variables to improve the agreement of model predictions with measurements in terms of waveforms.

We consider up to seven parameters: one parameter for the whole network, parameterizing the Young modulus of each vessel as $E = \theta_E E_{\text{orig}}$; peripheral compliance and resistance (two parameters for the whole network); four parameters related the inflow profile (systolic and backflow amplitudes, and systolic and backflow durations), see Figure 4, right.

Only two observational data are taken into account: flow at the thoracic aorta and pressure at the left radial artery. In order to assess the performance of the filter, and to compare with the estimation performed in time domain, we define the following estimation problems:

- (TD-CE), (FD-CE) Filter in time domain (TD) and in frequency domain (FD), only peripheral compliance and network Young modulus are estimated (filter in time domain and in frequency domain).

- (TD-CER) Filter in TD, peripheral compliance, network Young modulus and peripheral resistance are estimated.

- (FD-CE$_{>0}$) Filter in FD removing the first harmonic of measurements, peripheral compliance and network Young modulus are estimated.

- (FD-CEQ) Filter in FD, peripheral compliance, network Young modulus and inflow parameters are estimated.

- (FD-CEQ$_{>0}$) Filter in FD removing the first harmonic of measurements, peripheral compliance, network Young modulus and inflow parameters are estimated.

- (FD-CERQ) Filter in FD estimating the whole set of parameter.

- (FD-CERQ$_{>0}$) Filter in FD removing the first harmonic of measurements, peripheral compliance, network Young modulus, inflow parameters and peripheral resistance are estimated.

It is important to note that applying the filter in time domain does not allow to estimate parameters of the inflow curve, nor to exclude selected harmonics (i.e., the mean value) from the observations. Thus, these cases were not even considered.

Table 1 shows the effect of the filtered parameters for the different estimation settings in the error for the entire set of available measurements [22]. This investigation allows to assess to which extent the estimation, which is driven by minimizing the errors in two selected locations (bold columns in Table 1), influences the agreement of model prediction with measurements taken elsewhere in the network.

Case	lMCA-Q	lCCA-Q	lICA-Q	rECA-Q	abdAor-Q	**thoAor-Q**	**IRA-P**
Unfiltered	45.07	20.62	11.51	16.43	25.87	**10.71**	**18.70**
TD-CE	84.77	25.51	31.58	30.10	24.76	**10.70**	**19.16**
TD-CER	84.77	25.50	31.58	30.10	24.76	**10.70**	**29.16**
FD-CE$_{>0}$	57.59	19.19	16.22	16.68	23.90	**8.44**	**20.92**
FD-CE	57.38	19.19	16.11	16.65	23.91	**8.45**	**20.84**
FD-CEQ$_{>0}$	69.85	30.59	26.07	19.27	20.13	**0.72**	**14.29**
FD-CEQ	28.10	24.26	12.39	24.63	26.71	**1.30**	**15.81**
FD-CERQ$_{>0}$	43.43	26.72	17.67	17.18	22.28	**0.58**	**15.42**
FD-CERQ	54.11	28.15	20.90	16.52	20.21	**1.01**	**17.90**

Table 1: Average errors (Q: flow, P: pressure) in frequency domain for all available measurement points [22]. lMCA: left Middle Cerebral Artery; lCCA: left Common Carotid Artery; lICA: left Internal Carotid Artery; rECA: right External Carotid Artery; abdAor: abdominal Aorta; thoAor: thoracic Aorta; IRA: left Radial Artery.

The best results for the whole set of parameters are obtained in the setting FD-CERQ$_{>0}$. For this case, Figure 7 shows the variation of the seven parameters over time. One can see that the main changes are related to the inflow parameters, which appear to be the ones that influence the most the conformation of the pressure contour. The remaining parameters (network stiffness, capacitance and resistance of terminal vessels) remain almost unchanged. As in the previous test, most parameters converge after 50 iterations.
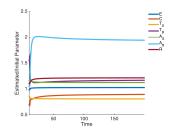

Figure 7: Test (FD-CERQ$_{>0}$). Values of the estimated parameters during the filter iteration (w.r.t. to the initial guesses).

Finally, Figure 8 shows that using the filtered parameters yields a considerable error reduction (with respect to unfiltered parameters) compared to the observation in the thoracic aorta, while the error reduction in the radial artery is smaller.

4.3 Discussion

The results of estimation based on in vivo measurements show that estimating the parameters in frequency domain leads to a more robust and more general procedure with respect to the estimation performed in the time domain. In our experience, the better performance (enhanced robustness
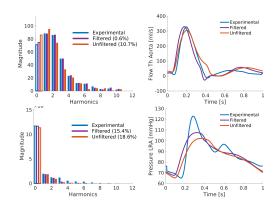
Figure 8: Test (FD-CERQ$_{>0}$). Left: Comparison of measurement, prediction before parameter estimation (unfiltered) and prediction after parameter estimation in frequency domain (error (17) shown in round brackets in the legend). Right: Comparison (in time domain) of measurements with simulation results using estimated parameters. The top row corresponds to the thoracic aorta, while the bottom row refers to the left radial artery.

and speed of convergence) of the estimation in frequency domain are due to the global information encoded in the different modes of cardiovascular signals. Hence, considering the measurements in frequency space provides the filter with information about the influence of parameters over the cardiovascular signals as whole inextricable unities. On the contrary, in time domain, the filter is influenced by the agreement (or disagreement) between the predicted variable and its measured value at particular instants in time.

A major drawback of the ROUKF in time domain is that it does not allow to consider tuning of inflow parameters (or, in general, any variable that parametrizes the *time profile* of boundary conditions). In fact, these parameters are highly variable in a patient-specific setting and they impact considerably the solution in the entire network, as reported in Table 1, which features a greater error reduction when inflow curve parameters were estimated. From the quantitative point of view, although the experimental setting is very challenging (few measurements, high uncertainty due to the unknown geometrical setting), the numerical results show that using the filtered parameters considerably reduces the error in frequency space in most vascular locations.

Furthermore, the robustness of the algorithm in frequency domain is enhanced by the possibility of pre-selecting the harmonics to be used for the estimation. Besides focusing on low frequencies (i.e., filtering the measurement data), this feature allows more robust estimation of parameters (such as the ones related to stiffnesses) mainly influencing the shape of the wave and not the average value (compare the errors for the settings FD-CERQ$_{>0}$ and FD-CERQ reported in Table 1).

5 Conclusion

We assessed the potential of the ROUKF in the frequency domain for parameter estimation in the context of one-dimensional blood flow models, considering real measurement data. Employing in vitro data, which implies reduced measurements and model uncertainty with respect to the real setting, the filtering in time and frequency domains have comparable accuracy. However, filtering in frequency space showed a faster convergence. In the case of in vivo measurements, the proposed algorithm broadens the possibilities of estimating model parameters that better characterize the observational

data. Indeed, our tests suggest that the estimation in frequency space offers advantages over the time domain counterpart, as it allows to focus on relevant harmonics, to eliminate errors due to gating of measurements and to estimate parameters related to boundary conditions, such as the ones that describe the waveform of a prescribed cardiac output.

The proposed strategy facilitates the translation of this kind of model inversion to realistic problems encountered in the clinic by focusing on global patient-specific features that better characterize cardiovascular signals.

Acknowledgment

References

[1] Alastruey, J., Khir, A.W., Matthys, K.S., Segers, P., Sherwin, S.J.: Pulse wave propagation in a model human arterial network: Assessment of 1-D visco-elastic simulations against *in vitro* measurements. Journal of Biomechanics **44**, 2250–2258 (2011)

[2] Bertoglio, C., Moireau, P., Gerbeau, J.F.: Sequential parameter estimation for fluid-structure problems. application to hemodynamics. Int. J. Numer. Meth. Biomed. Eng. **28**, 434–455 (2012)

[3] Blanco, P.J., Watanabe, S.M., Dari, E.A., Passos, M.R.F., Feijóo, R.A.: Blood flow distribution in an anatomically detailed arterial network model: criteria and algorithms. Biomech. Model Mechanobiol. **13**(6), 1303–1330 (2014)

[4] Blanco, P.J., Watanabe, S.M., Passos, M.R.F., Lemos, P.A., Feijóo, R.A.: An anatomically detailed arterial network model for one-dimensional computational hemodynamics. IEEE Transactions on Biomedical Engineering **62**(2), 736–753 (2015). DOI 10.1109/TBME.2014.2364522

[5] Boileau, E., Nithiarasu, P., Blanco, P.J., Müller, L.O., Fossan, F.E., Hellevik, L.R., Donders, W.P., Huberts, W., Willemet, M., Alastruey, J.: A benchmark study of numerical schemes for one-dimensional arterial blood flow modelling. International Journal for Numerical Methods in Biomedical Engineering pp. n/a–n/a (2015). DOI 10.1002/cnm.2732

[6] Caiazzo, A., Caforio, F., Montecinos, G., Müller, L., Blanco, P., Toro, E.: Assessment of reduced-order unscented Kalman filter for parameter identification in one-dimensional blood flow models using experimental data. Int. J. Numer. Methods Biomed. Engrg. **33**(8), e2843 (2016). DOI 10.1002/cnm.2843

[7] Formaggia, L., Quarteroni, A., Veneziani, A.: Cardiovascular Mathematics: Modeling and simulation of the circulatory system. Springer-Verlag Italia, Milano (2009)

[8] Huberts, W., Bode, A., Kroon, W., Planken, R., Tordoir, J., van de Vosse, F., Bosboom, E.: A pulse wave propagation model to support decision-making in vascular access planning in the clinic. Medical Engineering & Physics **34**(2), 233 – 248 (2012). DOI http://dx.doi.org/10.1016/j.medengphy.2011.07.015

[9] Julier, S.: The spherical simplex unscented transformation. In: Proc. of the American Control Conference, pp. 2430–4234 (2003)

[10] Julier, S., Uhlmann, J.: Unscented filtering and nonlinear estimation. Proceedings of the IEEE **92** (2004)

[11] Kalman, R., Bucy, R.S.: New results in linear filtering and prediction theory. ASME Trans. – Journal of Basic Engineering **83**(D), 95–108 (1961)

[12] Lal, R., Nicoud, F., Le Bars, E., Deverdun, J., Molino, F., Costalat, V., Mohammadi, B.: Non invasive blood flow features estimation in cerebral arteries from uncertain medical data. Ann. Biomed. Eng. **45**(11), 2574–2591 (2017). DOI 10.1007/s10439-017-1904-7

[13] Liang, F.Y., Fukasaku, K., Liu, H., Takagi, S.: A computational model study of the influence of the anatomy of the circle of willis on cerebral hyperperfusion following carotid artery surgery. BioMedical Engineering OnLine **10**(1), 84 (2011). DOI 10.1186/1475-925X-10-84

[14] Lombardi, D.: Inverse problems in 1D hemodynamics on systemic networks: a sequential approach. Int. J. Numer. Method Biomed. Eng. **30**(2), 160–179 (2014)

[15] Matthys, K.S., Alastruey, J., Peiró, J., Khir, A.W., Segers, P., Verdonck, P.R., Parker, K.H., Sherwin, S.J.: Pulse wave propagation in a model human arterial network: Assessment of 1-D numerical simulations against *in vitro* measurements. Journal of Biomechanics **40**, 3476–3486 (2007)

[16] Moireau, P., Chapelle, D.: Reduced-order Unscented Kalman Filtering with application to parameter identification in large-dimensional systems. Esaim Contr. Opt. Calc. Var. **17**, 380–405 (2011)

[17] Müller, L., Toro, E., Haacke, E., Utriainen, D.: Impact of CCSVI on cerebral haemodynamics: a mathematical study using mri angiographic and flow data. Phlebology (2015). DOI 10.1177/0268355515586526

[18] Müller, L.O., Blanco, P.J., Watanabe, S.M., Feijóo, R.: A high-order local time stepping finite volume solver for one-dimensional blood flow simulations: application to the ADAN model. International Journal for Numerical Methods in Biomedical Engineering pp. n/a–n/a (2016). DOI 10.1002/cnm.2761

[19] Müller, L.O., Toro, E.F.: Well-balanced high-order solver for blood flow in networks of vessels with variable properties. International Journal for Numerical Methods in Biomedical Engineering **29**(12), 1388–1411 (2013)

[20] Müller, L.O., Toro, E.F.: A global multiscale mathematical model for the human circulation with emphasis on the venous system. International Journal for Numerical Methods in Biomedical Engineering **30**, 681–725 (2014). DOI 10.1002/cnm.2622

[21] Mynard, J.P., Smolich, J.J.: One-dimensional haemodynamic modeling and wave dynamics in the entire adult circulation. Annals of Biomedical Engineering pp. 1–18 (2015). DOI 10.1007/s10439-015-1313-8

[22] Reymond, P., Bohraus, Y., Perren, F., Lazeyras, F., Stergiopulos, N.: Validation of a patient-specific one-dimensional model of the systemic arterial tree. American Journal of Physiology - Heart and Circulatory Physiology **301**(3), H1173–H1182 (2011). DOI 10.1152/ajpheart.00821.2010

[23] Safaei, S., Bradley, C.P., Suresh, V., Mithraratne, K., Muller, A., Ho, H., Ladd, D., Hellevik, L.R., Omholt, S.W., Chase, J.G., MÃijller, L.O., Watanabe, S.M., Blanco, P.J., de Bono, B., Hunter, P.J.: Roadmap for cardiovascular circulation model: Roadmap for cardiovascular circulation model. The Journal of Physiology (2016). DOI 10.1113/JP272660

[24] Toro, E.F.: Riemann Solvers and Numerical Methods for Fluid Dynamics: A Practical Introduction, third edn. Springer-Verlag (2009). ISBN 978-3-540-25202-3

[25] Toro, E. F. and Millington, R. and Nejad, L. A. M.: Towards very high order Godunov schemes. In: E.F. Toro (ed.) Godunov Methods. Theory and Applications, vol. 1, pp. 897–902. Kluwer/Plenum Academic Publishers, New York, Boston and London (2001). Conference in Honour of S K Godunov

[26] Wan, S., Van Der Merwe, R.: The unscented Kalman filter for nonlinear estimation. In: Adaptive systems for signal processing, communications, and control symposium, pp. 153–158 (2000)

[27] Xiao, N.: Simulation of 3D blood flow in the full systemic arterial tree and computational frameworks for efficient parameter estimation. Ph.D. thesis, Stanford University. Department of Bioengineering (2014)